Design of discrete and continuous super-resolving Toraldo pupils in the microwave range

LUCA OLMI[1,*], PIETRO BOLLI[1], AND DANIELA MUGNAI[2]

[1] Istituto Nazionale di Astrofisica (INAF), Osservatorio Astrofisico di Arcetri, Largo E. Fermi 5, I-50125 Firenze, Italy
[2] Consiglio Nazionale delle Ricerche (CNR), Istituto di Fisica Applicata Nello Carrara, Via Madonna del Piano 10, I-50019 Firenze, Italy
[*] Corresponding author: olmi.luca@gmail.com

Compiled January 12, 2018

The concept of super-resolution refers to various methods for improving the angular resolution of an optical imaging system beyond the classical diffraction limit. In optical microscopy several techniques have been successfully developed with the aim of narrowing the central lobe of the illumination Point Spread Function. In Astronomy, however, no similar techniques can be used. A feasible method to design antennas and telescopes with angular resolution better than the diffraction limit consists of using variable transmittance pupils. In particular, discrete binary phase masks (0 or π) with finite phase-jump positions, known as Toraldo Pupils, have the advantage of being easy to fabricate but offer relatively little flexibility in terms of achieving specific trade-offs between design parameters, such as the angular width of the main lobe and the intensity of sidelobes. In this paper we show that a complex transmittance filter (equivalent to a *continuous* Toraldo pupil, i.e., consisting of infinitely narrow concentric rings) can achieve more easily the desired trade-off between design parameters. We also show how the super-resolution effect can be generated with both amplitude- and phase-only masks and confirm the expected performance with electromagnetic numerical simulations in the microwave range. © 2018 Optical Society of America

OCIS codes: (100.6640) Superresolution; (050.1940) Diffraction; (110.6770) Telescopes; (350.1260) Astronomical optics

http://dx.doi.org/10.1364/ao.XX.XXXXXX

1. INTRODUCTION

The concept of super-resolution refers to various methods for improving the angular resolution of an optical imaging system beyond the classical diffraction limit. References [1] and [2] review and discuss the basic techniques for designing super-resolving pupil masks that use either *variable transmittance pupils* or phase masks for optical telescopes. The first time such variable transmittance pupils were discussed was at a lecture delivered by Toraldo di Francia at a colloquium on optics and microwaves in 1952[3]. Toraldo di Francia suggested that the classical limit of optical resolution could be improved interposing a filter consisting of either infinitely narrow concentric rings or finite-width concentric annuli of different amplitude and phase transmittance in the entrance pupil of an optical system. These pupils are now also known as Toraldo variable transmittance pupils (TPs, hereafter).

Discrete TPs (i.e., employing finite-width concentric coronae with different complex transmittance) have been widely analyzed in the context of microscopy[4–6], but so far they have never been applied to the design of telescopes or antennas with the goal of improving their nominal angular resolution. The first proof-of-principle laboratory results of a super-resolving lens-collimator optical system, mimicking a telescope configuration, employing a binary phase plate has been recently published[7]. This work confirms the potential of variable transmittance pupils as a tool to achieve super-resolution with a telescope-like optical system.

The first experimental studies in the microwave range of a discrete TP were carried out in 2003[8] and 2004[9]. More recently, we have carried out a series of extensive electromagnetic (EM) numerical simulations using the commercial software FEKO[1], a comprehensive EM simulation software tool for the electromagnetic field analysis of 3-D structures[10]. We have then used these EM simulations to prepare more comprehensive laboratory tests at 20 GHz involving different types of discrete TPs, which are extensively discussed elsewhere[11]. This preliminary work confirms that discrete TPs can yield the super-resolution effect, both in the **near-field (NF) and far-field (FF)**, and suggest that TPs could represent a viable approach to achieve super-resolution in Radio Astronomy.

The gain in angular resolution, however, is accompanied by two undesirable side effects: the loss of efficiency and increased sidelobes level. For astronomical observations the

[1] http://www.altairhyperworks.com/product/FEKO

loss of efficiency represents the most unfavorable situation, but in practice it can be mitigated by a trade-off between all these performance indicators. In addition, the use of mesh filters[22] to implement TPs could further reduce the loss of efficiency. However, we note that the ability of TPs to engineer the Point Spread Function (PSF) is not necessarily limited to applications where super-resolution is required but, for example, TPs could also be used to significantly decrease ($\lesssim -50$ dB) the level of the sidelobes, as required by measurements of the Cosmic Microwave background (see, e.g., Ref. [23]). At present, we are interested in the realization of a proof-of-concept TP prototype capable of achieving super-resolution for radio astronomical applications, but not yet optimized in terms of efficiency and sidelobes strength.

Our previous EM simulations and experimental measurements[10, 11] indicate that increasing the number of finite-width coronae of the TP allows to achieve more easily a reasonable trade-off between the width of the central lobe and the strength of the sidelobes. Hence, it is of interest to analyze the design parameter-space of a TP consisting of infinitely narrow concentric rings, or a *continuous* Toraldo pupil. Therefore, in Sect. 2 we first show that, as expected on the basis of the theory of diffraction, the FF generated by a continuous TP is mathematically equivalent to that described by the Fraunhofer diffraction integral. In Sect. 3 we then show that the formalism derived for the continuous TP can also be used to analyze the discrete TPs, and we also analyze the performance of the continuous TP. In particular, we compare two examples of continuous amplitude- and phase-only filters. Then, in Sect. 4 we describe a FEKO numerical simulation of a simple continuous phase-only mask. We finally draw our conclusions in Sect. 5

2. DERIVATION OF THE FAR-FIELD FOR THE CONTINUOUS TORALDO PUPIL

A. The discrete Toraldo Pupil

We begin this section by briefly reviewing the theory of discrete TPs. Following Toraldo di Francia[3] let us consider a circular pupil of diameter D and divide it into n circular coronae of finite width by means of $n+1$ circumferences with diameters $\rho_0 D$, $\rho_1 D$, ..., $\rho_n D$, where ρ_0, ..., ρ_n is a succession of numbers in increasing order, with $\rho_0 = 0$ and $\rho_n = 1$. This is what we call the *discrete* Toraldo pupil. By setting $x = \pi \frac{D}{\lambda} \sin\theta$, where θ is the angle of diffraction measured with respect to the optical axis and λ is the wavelength, it can be shown that the total FF amplitude, $A_{\rm tot}(x)$, diffracted by the discrete TP is given by:

$$A_{\rm tot}(x) = \sum_{i=0}^{n-1} \frac{k_{i+1}}{x} [\rho_{i+1} J_1(\rho_{i+1} x) - \rho_i J_1(\rho_i x)] = \sum_{i=0}^{n-1} F(x;\rho,k) \quad \textbf{(1)}$$

where $k_{i+1} = \frac{\pi D^2}{2\lambda^2} A_{i+1}$ is a constant that is proportional to the amplitude A_{i+1} illuminating uniformly each corona, and J_1 is the Bessel function of the first order. Once the partition of the pupil into a number of circular coronae is established, we can impose n independent conditions on Eq.(1) (for instance, the x values of its zeros), thus obtaining a system of n equations from which we can determine the coefficients $k_1, ..., k_n$. Note that the k_i coefficients can also have negative values, in which case they represent a *phase-inversion* of the wave propagating through the pupil (see Sect. B).

Let us now consider the simple case of a three-coronae TP with the radii in arithmetic progression, $\rho_0 = 0$, $\rho_1 = 1/3$,

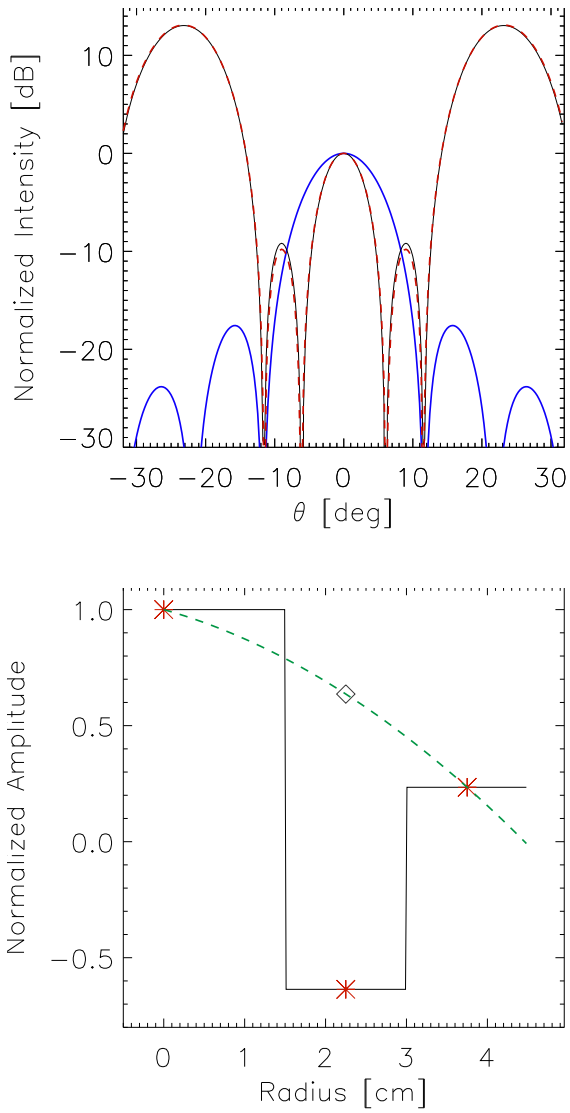


Fig. 1. *Top panel.* Diffraction pattern at $\nu = 20$ GHz by a 3-coronae TP, as given by the square of Eq.(1) for $n = 3$ (black solid line), and that of an open pupil of equal diameter (blue solid line). The red dashed line, almost exactly overlapping with the black solid line, represents the diffracted amplitude as obtained by Eq. (8) using the input illumination shown in the bottom panel. All curves are normalized with respect to the on-axis value. *Bottom panel.* Pupil illumination for a 3-coronae TP, with a 9 cm diameter, as required by Eq.(1). The "*" symbols represent the relative magnitudes of the coefficients k_1, k_2 and k_3, while the dashed green line represents the 2^{nd}-order polynomial best-fit to the three points. The black solid line represents the ideal entrance pupil illumination, as given by Eq.(1), where the amplitude of the illumination is uniform over each separate corona. A negative amplitude in the middle corona indicates a phase inversion.

$\rho_2 = 2/3$ and $\rho_3 = 1$ and a diameter of 9 cm (see ref. [8]). As discussed in the previous section, if for example we set the following three conditions[8] $A(x=0)=1$, $A(x=2)=0$ and $A(x=3.8)=0$, we find that $k_1 = 68.3$, $k_2 = -43.4$ and $k_3 = 16.0$. Then, Fig. 1 shows the diffracted intensity and required illumination for this TP. The figure shows the reduction (by a factor of $\simeq 2.5$) of the central lobe for the TP compared to the open pupil, accompanied by a significant increase in the intensity of the sidelobes. The bottom panel of Fig. 1 shows the pupil (amplitude) illumination required by the k-coefficients. As far as the phase is concerned, the illumination of a TP requires a uniform phase (i.e., a plane wave) except on those coronae with negative k-coefficients, which require a phase inversion. A discrete TP can then be considered a binary phase mask (0 or π) with finite phase-jump positions.

The 3-coronae TP can be considered the first step in analyzing and developing more efficient discrete TPs (see Sect. A). At microwave wavelengths it is easy to fabricate and relatively easy to study experimentally. A description of full electromagnetic numerical simulations of both 3- and 4-coronae TPs can be found in ref. [10] while a complete description of laboratory measurements of these simple TPs can be found in ref. [11]. These works show that the use of a larger number of coronae allows to achieve a better trade-off between specific design parameters, such as the width of the main lobe and the level of the sidelobes, which can be quite high, as shown in Fig. 1 for the simple example of the 3-coronae TP. It is therefore of interest to analyze the properties of TPs with large numbers of narrow concentric coronae and, in particular, the limit for inifinitely narrow concentring rings, i.e. a *continuous* TP.

B. The continuous Toraldo Pupil

We now want to show that Eq.(1) becomes equal to the classic Fraunhofer diffraction formula when the number of coronae is progressively increased and their width becomes infinitesimally small. In order to do this, let us assume that the number of coronae is sufficiently large that if we write $\rho_i = r_i/R$, where r_i is the radius of the i-th corona and $R = D/2$, then the coefficient ρ_{i+1} can be written as:

$$\rho_{i+1} = \frac{r_i + \Delta r}{R} = \rho_i + \frac{\Delta r}{R} \tag{2}$$

If in addition we write $k_i \to k(r)$ and $k_{i+1} \to k(r+\Delta r)$ then we can write the function $F(x;\rho,k)$ in Eq.(1) as:

$$F(x;\rho,k) \quad \to \quad F(x;r,\Delta r,k) = \frac{k(r+\Delta r)}{x} \times \left[\frac{r+\Delta r}{R} J_1\left(\frac{r+\Delta r}{R}x\right) - \frac{r}{R} J_1\left(\frac{r}{R}x\right)\right].$$

If we now define a new variable, $z(r) = \frac{r}{R}x = \rho\, x$ and assume that $\Delta r \ll r$, then we can approximate the Bessel functions in Eq.(3) as:

$$J_1\left(\frac{r+\Delta r}{R}x\right) = J_1(z+\Delta z) \simeq J_1(z) + \Delta z J_1' \tag{3}$$

where $J_1'(z) \equiv \frac{\mathrm{d}J_1(z)}{\mathrm{d}z}$. Then using the fundamental relation[12]:

$$J_1'(z) = J_0(z) - \frac{1}{z} J_1(z) \tag{4}$$

we can also write:

$$J_1(z+\Delta z) \simeq J_1(z)\left(1 - \frac{\Delta z}{z}\right) + \Delta z\, J_0(z)\,. \tag{5}$$

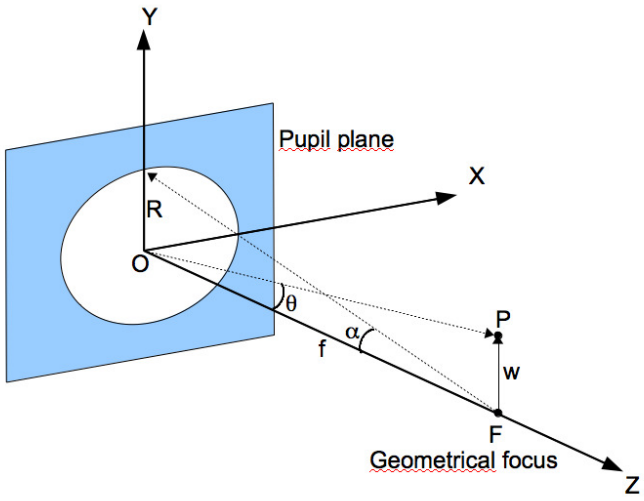


Fig. 2. Illustration of the notation used in determining Eq.(9). P is a point near the focus, F, f is the focal length, and R is the pupil radius. w represents the radial coordinate in the focal plane.

Substituting this back into Eq.(3) we then obtain:

$$F(x;r,\Delta r,k) \simeq \frac{k(r+\Delta r)}{z^2}\left(\frac{r}{R}\right)^2 \times \left[z\Delta z J_0(z) + (\Delta z)^2\left(J_0(z) - \frac{J_1(z)}{z}\right)\right],$$

and neglecting the 2nd-order term[2] we finally obtain:

$$F(x;r,\Delta r,k) \simeq \frac{k(r+\Delta r)}{R^2} J_0\left(\frac{r}{R}x\right) r\,\Delta r \tag{6}$$

where we can also write:

$$k(r+\Delta r) \simeq k(r) + \Delta r\, k'(r)\,. \tag{7}$$

For sufficiently small values of Δr the summation in Eq.(1) can be replaced with an integral. Therefore, after substituting Eq.(7) in Eq.(6) and neglecting once again the 2nd-order term, the result can be used to write Eq.(1) in integral form as:

$$A_{\mathrm{tot}}(x) = \frac{2\pi}{\lambda^2}\int_0^R A(r) J_0\left(\frac{r}{R}x\right) r\,\mathrm{d}r = \frac{2\pi R^2}{\lambda^2}\int_0^1 A(\rho) J_0(\rho x)\rho\,\mathrm{d}\rho \tag{8}$$

where we have also used $k(r) = \frac{\pi D^2}{2\lambda^2} A(r)$. We can see that Eq.(8), except for a normalization constant, is equal to the Fraunhofer diffraction integral[13], which allows to calculate the diffracted amplitude as a function of angle θ if we know the *continuous* amplitude distribution, $A(r)$, over the pupil. Toraldo di Francia, describing the diffraction by a circular aperture, also derived a similar result in his book[14].

Eq.(8) can be easily shown to also give the amplitude in the focal region of a converging monochromatic spherical wave front passing through the center of the pupil and focused by a (thin) lens of focal length f placed after the pupil. In fact, if we indicate with w the radial coordinate in the focal region, then we have $\tan\theta = w/f$ (see Fig. 2). If we are only interested to

[2] At $z = 0$ the second-order term is $\propto (\Delta z)^2$.

a region near the optical axis, then $w/f = \tan\theta \simeq \sin\theta$. We also introduce the numerical aperture of the lens, NA$= \sin\alpha \simeq \tan\alpha = R/f$, where α represents the angle, as measured from the lens focus, that subtends the radius R of the pupil, and we have also assumed that NA is small. Then, in Eq.(8) we can write $\rho x = k_\lambda R\rho \sin\theta = \rho\, k_\lambda \mathrm{NA}\, w$, where $k_\lambda = 2\pi/\lambda$. Finally, defining the radial dimensionless optical coordinate at the focus $v = k_\lambda\, \mathrm{NA}\, w$ we can rewrite Eq.(8) as:

$$A_{\mathrm{tot}}(v) \propto \int_0^1 A(\rho) J_0(v\rho)\rho\, \mathrm{d}\rho \qquad \textbf{(9)}$$

which gives the amplitude of the converging wave in the focal region[13].

Both Eqs.(8) and (9) are valid when the amplitude illumination function, $A(r)$, is replaced with a complex pupil function of type $\hat{A}(r) = A(r)\, \exp[j\phi(r)]$, where now $A(r)$ represents the transmittance function, and $\phi(r)$ is the phase function. This feature is implicitly contained in the original work by Toraldo di Francia[3], since the negative k coefficients of Eq.(1) correspond to $\phi = \pi$, i.e., represent a phase inversion of the incident wave, as previously mentioned in Sect.A.

3. PERFORMANCE OF CONTINUOUS TORALDO PUPIL

A. Application to the discrete 3-coronae Toraldo Pupil

As an example of application of the continuous TP, we have applied Eq.(8) to the case of the simple 3-coronae TP described in Sect. 2A. The amplitude of the illumination function for the continuous TP, $A(r)$ in Eq.(8), has been set proportional to the step-like normalized amplitude shown in the bottom panel of Fig. 1 (solid line). Then, the diffracted FF amplitude has been computed through Eq.(8), and the resulting intensity $\propto A_{\mathrm{tot}}^2$, is shown in the top panel of Fig. 1 as the red dashed line. The same illumination amplitude has been used to calculate the diffracted FF amplitude of the discrete TP, as given by Eq.(1), and shown in Fig. 1 as the black solid line. Both lines can be compared with the intensity diffracted by the open pupil, shown by the blue solid line in the top panel of Fig. 1.

One can note the extreme similarity of the diffracted intensity as obtained by either the discrete or continuous TP. The two curves are not *exactly* equal, and we think that the small residual difference is likely a combined effect of both the intrinsic approximations used to get Eq.(8) and the accuracy of the numeric simulation. However, at present we have not further investigated this discrepancy. Figure 1 also shows how the reduction in the angular width of the central lobe is accompanied by a huge rise in the relative intensity of the far sidelobes. In the Optics literature one is usually concerned about the trade-off between the normalized spot size, G (also known as the resolution gain or G-factor), defined as the ratio between the half-width at the half-maximum (HWHM) of the super-resolved pattern and the HWHM of the Airy disk pattern, and the on-axis Strehl ratio, S, defined as the ratio between the intensity of the super-resolved pattern and the intensity of the Airy disk pattern (see, e.g., ref. [16]). For example, in scanning microscopy the position and intensity of the highest sidelobes set the limit to the usable field of view. In Astronomy, however, the sidelobes level and overall efficiency also represent important parameters of the optimization procedure.

B. Example of continuous amplitude-only filter

We now consider a pupil with a continuous, amplitude-only, aperture illumination, i.e., $\hat{A}(r) = A(r)$. If this function is

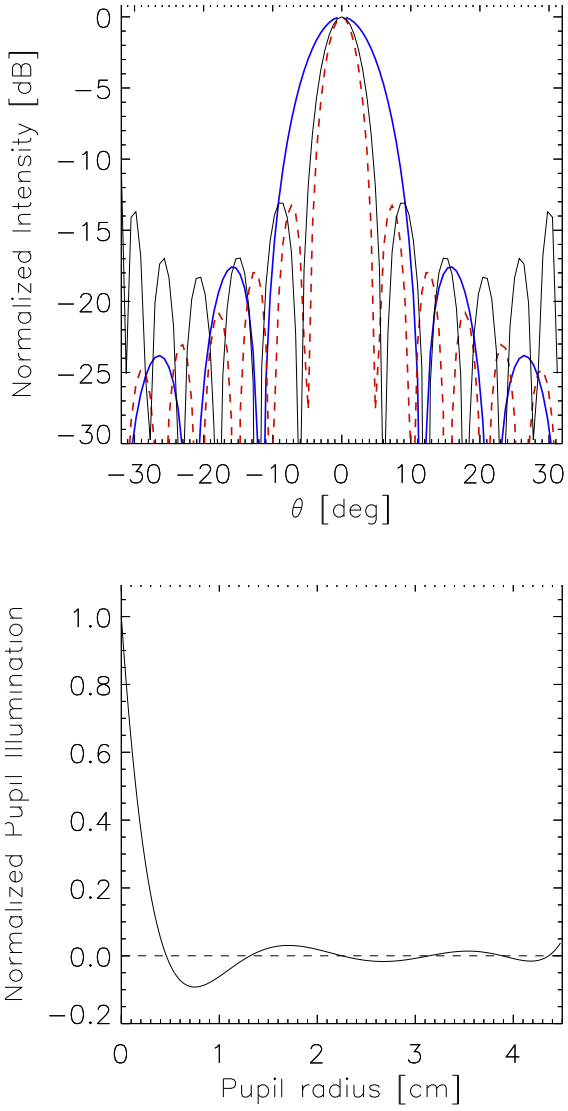


Fig. 3. *Top panel.* Diffraction pattern at $\nu = 20$ GHz by a continuous TP. The red dashed line represents the desired intensity in the FF, as obtained by using a $sinc^2$ function. The black solid line represents the best-fit diffraction pattern, obtained using Eq.(8) and solving for the aperture illumination, $A(r)$. The blue solid line is the same as in Fig. 1, and all curves are normalized with respect to the on-axis value. *Bottom panel.* Pupil illumination of the continuous TP, $A(r)$, as obtained from a best-fit procedure applied to Eq.(8). As before, a negative amplitude indicates a phase inversion.

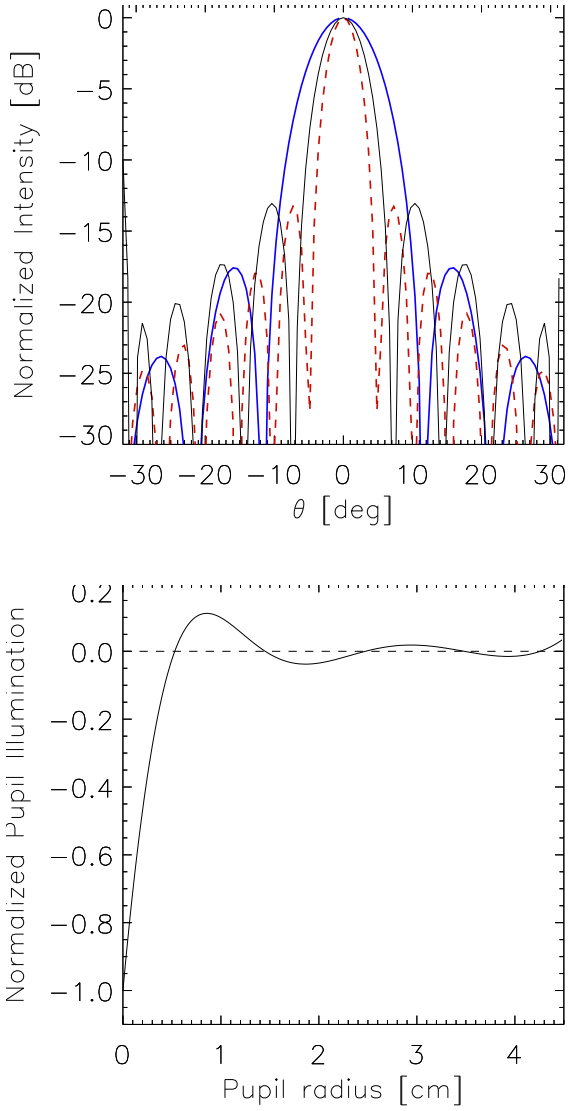


Fig. 4. Same as Fig. 3, but using as aperture illumination, $A(r)$, the linear combination of a Gaussian function and a polynomial.

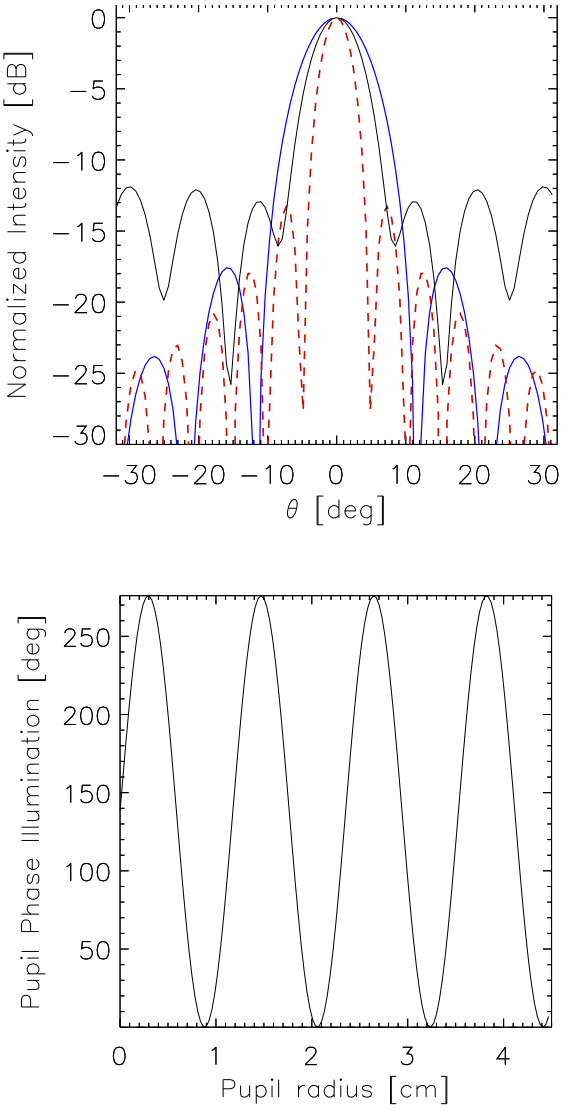


Fig. 5. Same as Fig. 3, but using a phase-only aperture illumination, i.e., $\hat{A}(r) = \exp[j\phi(r)]$. In this case the phase function, $\phi(r)$, shown in the bottom panel, was a simple sine function.

known then it is easy to calculate the diffracted amplitude from Eq.(8). However, we will follow instead the inverse procedure, where a desired diffracted amplitude, $A_{\rm tot}$, is set, and the required aperture illumination is then derived. This is similar to various methods proposed in the literature which aim to optimize the design of the super-resolving filter given a set of constraints, one of which is usually the resolution gain G. **The algorithm that we have implemented compares the desired diffracted amplitude, $A_{\rm tot}$, with that obtained by applying Eq.(8) using a given aperture illumination (e.g., polynomial) and a specific set of parameters (e.g., the polynomial coefficients) that can be modified by a minimization procedure (in our case we used the `MPFIT` function [17] for the IDL software[18]) until a satisfactory match is found.**

In the example discussed here, the desired diffracted amplitude has been derived using a standard *sinc* function and we imposed a resolution gain $G = 0.44$. The resulting normalized intensity, $\propto A_{\rm tot}^2$ as in the previous example, is shown as the red dashed line in the top panel of Fig. 3, and can be compared with the usual normalized diffracted intensity by an open pupil with the same diameter (blue solid line). If $A_{\rm tot}$ is set, then Eq.(8) can be used to solve for the required aperture illumination, $A(r)$. The functional form of $A(r)$ chosen for this specific example was a $6^{\rm th}$-order polynomial. The bottom panel in Fig. 3 shows the optimized $A(r)$, while the black solid line in the top panel shows the best-fit diffracted intensity, as obtained from the polynomial $A(r)$ using Eq.(8). One can note that the best-fit for the intensity, $I_{\rm tot} = A_{\rm tot}^2$ reproduces quite well the desired FF beam up to the first sidelobes, but discrepancies increase at larger angular distances from the optical axis. **In fact, we note that the required full width at half maximum, FWHM, i.e. at -3 dB from the peak, is achieved within $\lesssim 1$ deg, and also the first sidelobe intensity is the same within $\lesssim 0.5$ dB. The positions of the sidelobes do not coincide with those of the original reference beam, but for most astronomical observations this effect is less significant compared to the sidelobe strength.**

We have used other functional forms for the aperture illumination, such as the linear combination of a Gaussian function and a polynomial, or Gaussian and sine functions. Our results indicate that the optimized $A(r)$ still resembles the basic shape shown in Fig. 3, i.e., with a central peak followed by a series of secondary maxima and minima. We note that in this case the level of the sidelobes is already much reduced, **by $\simeq 3$ dB**, compared to the simple discrete TP analyzed in Fig. 1. It is however possible to achieve a different trade-off between the G-factor and the intensity of the sidelobes, as shown in Fig. 4. In fact, in this case G has increased (i.e., we have a *lower* super-resolution effect, by $\lesssim 20\,\%$), but the sidelobes are now decreasing far from the optical axis. This example shows that, independently of the selected functional form of the aperture illumination, the resulting shape of the optimized $A(r)$ would be very difficult to implement in practice, especially at microwave wavelengths. It is therefore of interest to analyze, in the next section, the case of phase-only masks.

C. Example of continuous phase-only filter

We now replace the amplitude illumination function, $A(r)$, with a phase-only pupil function of type $\hat{A}(r) = \exp[j\phi(r)]$, and proceed as before by setting the required FF amplitude, $A_{\rm tot}$, and then finding the best-fit phase function, $\phi(r)$, using the `MPFIT` optimization procedure. As an example of this procedure, in Fig. 5 we show the calculated FF when the phase function is a

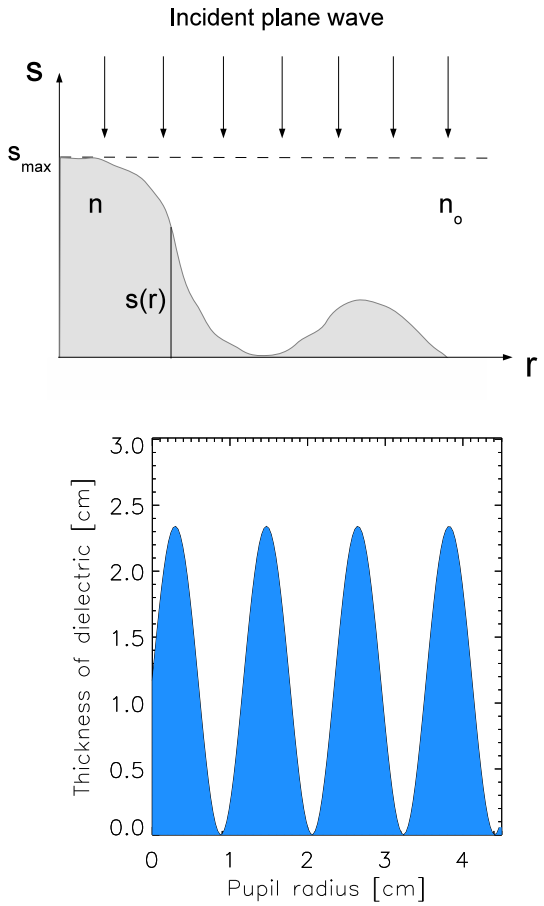


Fig. 6. *Top panel.* Parameters used in the description of the phase-only pupil. *Bottom panel.* The phase illumination converted into a phase mask at $\nu = 20$ GHz. The mask shows the required thickness variations in a dielectric material with a refraction index $\simeq 1.5$.

sine function of type $\phi(r) = a\frac{\pi}{2}[1+\sin(br)]$ (see also Sect. 4), where the parameters a and b are determined by the optimization procedure. The best-fit result for the diffraction pattern is shown by the black solid line, which can be compared with the input, specified pattern (red dashed line) and also with the usual normalized diffracted amplitude by an open pupil with the same diameter (blue solid line). The best-fit phase function can be converted into the equivalent thickness of a dielectric plate, as described later in Sect. 4.

The discrepancy between the input and best-fit diffraction patterns is now larger compared with that of the examples discussed in Sect. 3B, as previously shown in Figures 3 and 4 **(the resulting FWHM is now larger by $\gtrsim 50\,\%$ compared to the input value).** Clearly, we have analyzed only a few representative cases, for both amplitude- and phase-only illumination, and thus the comparison presented here between these few examples should not be considered final. However, while an arbitrary amplitude-only illumination is very difficult to implement in practice, as noted earlier, a phase-only illumination can be easily converted into a phase mask, as shown in the bottom panel of Fig. 6.

These masks could be easily manufactured using computer numerical control milling machines (CNC), which enable to produce the phase filters from their digitized 3D description, by automatically excavating the object shape from a block of raw dielectric material, whose variable thickness is described in the next section. However, we are currently investigating the possibility to use mesh filters[22] to fabricate the continuous phase masks. Finally, since finding the most effective global optimization method is out of the scopes of this work, as we mentioned earlier we have used the readily available IDL optimization procedure `MPFIT`. However, a variety of global optimization methods have been tested with different types of pupil masks, which include, e.g., simulated annealing [19] as well as various versions of the genetic algorithm [20, 21].

4. EM NUMERICAL SIMULATION OF A CONTINUOUS TORALDO PUPIL

A. Determination of the thickness profile for a continuous phase-only filter

In Sect. 1 we mentioned the EM numerical simulations of discrete TPs conducted with FEKO and discussed elsewhere[10]. We therefore modified one of our previous FEKO simulations to model a continuous phase-only pupil, and specifically the example discussed in Sect. 3C. This new model required the conversion of the optimized phase-only transmittance radial profile into an equivalent thickness profile of a slab of dielectric material. The relation between the phase-delay introduced by the phase-only pupil function and the thickness profile of a shaped slab of dielectric material, with uniform refraction index n, is illustrated in Fig. 6. Assuming that $s(r)$ represents the physical profile of the dielectric material and $l(r)$ represents the optical path length (OPL), with $l(r) = n\,s(r)$, then Fig. 6 shows that the minimum OPL occurs when $l_o = n_o\,s_{\max}$, and the maximum value is $l_{\max} = n\,s_{\max}$, assuming that the refraction index of the dielectric material is larger than the refraction index of the surrounding medium, n_o. Then, the optical path *excess*, $\Delta l(r) = l(r) - l_o$, between a ray through the dielectric medium at radial position r and a ray that does not intercept the

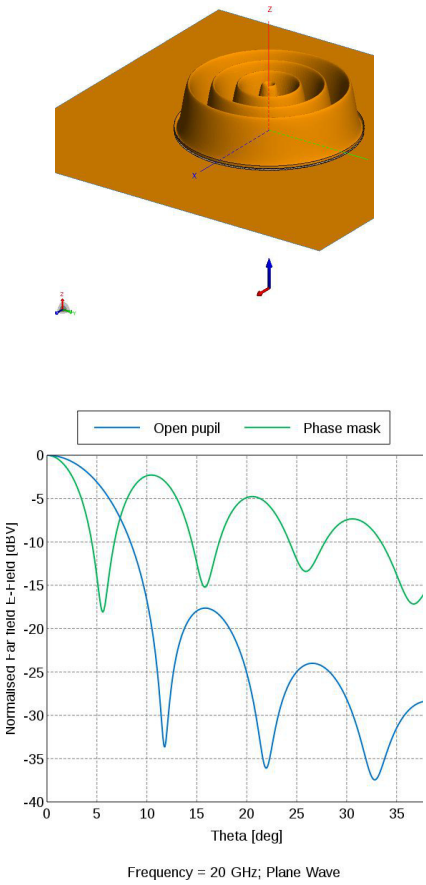


Fig. 7. *Top panel.* FEKO 3D model to implement the phase-only pupil. The dielectric material composing the pupil has a refraction index $n = 1.5$, and the pupil aperture is realized in an infinite ground-plane. The arrows below the pupil show the direction of incidence of a plane wave (blue arrow), and also the direction of the linear polarization (red arrow). *Bottom panel.* FF results from the FEKO simulation at $\nu = 20\,\mathrm{GHz}$, normalized to the on-axis value.

medium is:

$$\Delta l(r) = \{ns(r) + n_o[s_{\max} - s(r)]\} - n_o s_{\max} = (n - n_o)s(r) \quad (10)$$

with $0 \le s(r) \le s_{\max}$. Given that the phase delay introduced by the optical path excess is $\phi(r) = k\,\Delta l(r)$, where k is the wavenumber (not to be confused with the coefficients k_i defined in Sect. A), then we have:

$$s(r) = s_{\max}\frac{\phi(r)}{2\pi} \quad (11)$$

with $s_{\max} = \lambda/(n - n_o)$, and $0 \le \phi(r) \le 2\pi$. The example shown in Fig. 5 then corresponds to the phase function $\phi(r) = a\frac{\pi}{2}[1 + \sin(br)]$, where $a = 1.533$ and $b = 5.342\,\mathrm{cm}^{-1}$. This phase function results in the thickness profile shown in the bottom panel of Fig. 6. **In the microwave range these phase masks are easy to fabricate with CNC techniques since the tolerance required on the thickness is $\lesssim 1$ mm for phase variations < 1 deg.**

B. Results of the FEKO simulation

Once the thickness profile of the dielectric material composing the phase filter was determined, we imported the shaped transmittance pupil in the FEKO model, as shown in the top panel of Fig. 7. The pupil was illuminated by a plane wave, with a specific polarization, and the resulting FF diffracted by the pupil was evaluated. This is shown in the bottom panel of Fig. 7, where the blue curve represents the FF by the open pupil, whereas the green curve represents the diffracted field by the continuous phase pupil. Both curves are normalized to their on-axis value so that it is easier to detect any super-resolution effect. One can then see the usual behaviour of a TP, with a narrower main beam and higher sidelobes, similar but not quite the same as the analytical result previously shown in Fig. 5, where the resulting sidelobes are somewhat lower compared to the FEKO simulated FF. A likely explanation, at least partially, for this discrepancy is the fact that while the result shown in Fig. 5 is based on a 2-D pupil, FEKO simulates the actual 3-D structure of the shaped dielectric material which, as shown in the bottom panel of Fig. 6, significantly differs from an idealized optically thin phase filter.

5. CONCLUSIONS

As a follow-up to our recent EM simulations and experimental measurements of discrete Toraldo Pupils [10, 11], i.e. consisting of finite-width concentric coronae of different amplitude and binary phase transmittance (0 or π), we have analyzed several cases of both discrete and continuous TPs for the specific case of the microwave range, which is of interest for radio astronomical applications. We have shown that the continuous TP, corresponding to the limiting case of a discrete TP when the finite coronae become infinitely narrow concentric rings transforms, generates a far-field equivalent to that described by the Fraunhofer diffraction integral for a complex transmittance filter. We have shown that the formalism derived for the continuous TP can also be used to analyze the classical discrete TP. Compared to the discrete TP, the continuous TP has a wider design parameter-space, and thus can more easily achieve a specific trade-off between several design parameters, such as the width of the central lobe and the strength of the sidelobes.

We have also applied the concept of continuous TP to the limiting cases of amplitude- and phase-only masks. The latter is the only one that can be easily fabricated for applications in the microwave range, and we have shown that even very simple phase masks can yield the super-resolution effect while ensuring relatively low-level sidelobes. We have used a general purpose optimization IDL procedure, but more complex global optimization algorithm should be able to yield design parameters closer to the desired ones. An EM numerical simulation conducted with the software FEKO confirms that the super-resolution effect can be obtained with a simple phase mask, though the sidelobe levels are higher than predicted by the analytical model.

6. FUNDING INFORMATION

We gratefully acknowledge the contribution of the Ente Cassa di Risparmio di Firenze (Italy) for supporting this research (grant 2015.0927A2202.8861).

REFERENCES

1. M. P. Cagigal, V. F. Canales, and J. E. Oti, "Design of Continuous Superresolving Masks for Ground-based Telescopes", Publications of the Astronomical Society of the Pacific **116**, 965 (2004)
2. V. F. Canales, D. M. de Juana and M. P. Cagigal, "Superresolution in compensated telescopes", Optics Letters **29**, 935 (2004)
3. G. Toraldo di Francia, "Nuove pupille superrisolventi", Atti Fond. Giorgio Ronchi **7** (1952)
4. M. A. A. Neil, T. Wilson and R. Juskaitis, "A wavefront generator for complex pupil function synthesis and point spread function engineering", Journal of Microscopy **197**, 219 (2000)
5. M. Martinez-Corral, M. T. Caballero, E. H. K. Stelzer and J. Swoger, "Tailoring the axial shape of the point spread function using the Toraldo concept", Optics Express **10**(1), 98 (2002)
6. H. Kim, G. W. Bryant and S. J. Stranick, "Superresolution four-wave mixing microscopy", Optics Express **20**, 6042 (2012)
7. C. Wang, D. Tang, Y. Wang, Z. Zhao, J. Wang, M. Pu, Y. Zhang, W. Yan, P. Gao, X. Luo, "Super-resolution optical telescopes with local light diffraction shrinkage", Nature Scientific Reports, **5**, id.18485 (2015)
8. D. Mugnai, A. Ranfagni and R. Ruggeri, "Pupils with super-resolution", Physics Letters A **311**, 77 (2003)
9. A. Ranfagni, D. Mugnai and R. Ruggeri, "Beyond the diffraction limit: Super-resolving pupils", Journal of Applied Physics **95**, 2217 (2004)
10. L. Olmi, P. Bolli, L. Cresci, D. Mugnai, E. Natale, R. Nesti, D. Panella and L. Stefani, "Super-resolution with Toraldo pupils: analysis with electromagnetic numerical simulations", Proc. of SPIE, Volume 9906, Astronomical Telescopes and Instrumentation (2016)
11. L. Olmi, P. Bolli, L. Cresci, F. D'Agostino, M. Migliozzi, D. Mugnai, E. Natale, R. Nesti, D. Panella and L. Stefani, "Laboratory measurements of super-resolving Toraldo pupils for radio astronomical applications", Experim. Astron., **43**, 285 (2017)
12. `http://mathworld.wolfram.com/BesselFunctionoftheFirstKind.html`
13. M. Born and E. Wolf, "*Principles of Optics*" (Cambridge University Press, 1999)
14. G. Toraldo di Francia "*La diffrazione della luce*" (Einaudi, 1958)
15. I. J. Cox, C. J. R. Sheppard and T. Wilson, "Reappraisal of arrays of concentric annuli as superresolving filters", Journal of the Optical Society of America **72**(9), 1287 (1982)
16. T. R. M. Sales and G. M. Morris, "Fundamental limits of optical supreresolution", Optics Letters **22**(9), 582 (1997)
17. C. B. Markwardt, in Astronomical Society of the Pacific Conference Series, Vol. 411, Astronomical Data Analysis Software and Systems XVIII, ed. D. A. Bohlender, D. Durand, & P. Dowler, 251 (2009)
18. `http://www.exelisvis.com/ProductsServices/IDL.aspx`
19. L. Liu and G. Wang, "Designing superresolution optical pupil filter with constrained global optimization algorithm", Optik **119**,481–484 (2008)
20. L. N. Hazra and N. Reza, "Optimal design of Torald super resolving filters", Proc. of SPIE, Vol. 7787 (2010)

21. D. M. de Juana, J. E. Oti, V. F. Canales, and M. P. Cagigal, “Design of superresolving continuous phase filters”, Optics Letters **28**(8), 607 (2003)
22. G. Pisano, M. W. Ng, F. Ozturk, B. Maffei and V. Haynes, "Dielectrically embedded flat mesh lens for millimeter waves applications", Applied Optics **52**(11), 2218 (2013)
23. M. Bersanelli, E. Mattaini, E. Santambrogio, A. Simonetto, S. Cirant, F. Gandini, C. Sozzi, N. Mandolesi and F. Villa, "A Low-Sidelobe, High Frequency Corrugated Feed Horn for CMB Observations", Experimental Astronomy **8**(3), 231 (1998)